Adsorption-Controlled Growth of $BiFeO_3$ by MBE and Integration with Wide Band Gap Semiconductors

Jon F. Ihlefeld, Wei Tian, Zi-Kui Liu, W. Alan Doolittle, Margitta Bernhagen, Peter Reiche, Reinhard Uecker, Ramamoorthy Ramesh, and Darrell G. Schlom

***Abstract*—$BiFeO_3$ thin films have been deposited on (001) $SrTiO_3$, (101) $DyScO_3$, (011) $DyScO_3$, (0001) AlGaN/GaN, and (0001) 6H-SiC single crystal substrates by reactive molecular beam epitaxy in an adsorption-controlled growth regime. This is achieved by supplying a bismuth over-pressure and utilizing the differential vapor pressures between bismuth oxides and $BiFeO_3$ to control stoichiometry in accordance with thermodynamic calculations. Four-circle x-ray diffraction and transmission electron microscopy reveal phase-pure, epitaxial films with rocking curve full width at half maximum values as narrow as 7.2 arc seconds (0.002°). Epitaxial growth of (0001)-oriented $BiFeO_3$ thin films on (0001) GaN, including AlGaN HEMT structures, and (0001) SiC has been realized using intervening epitaxial (111) $SrTiO_3$ / (100) TiO_2 buffer layers. The epitaxial $BiFeO_3$ thin films have 2 in-plane orientations: [11$\bar{2}$0] $BiFeO_3$ || [11$\bar{2}$0] GaN (SiC) plus a twin variant related by a 180° in-plane rotation. This epitaxial integration of the ferroelectric with the highest known polarization, $BiFeO_3$, with high bandgap semiconductors is an important step toward novel field-effect devices.**

I. Introduction

Recently there has been increased interest in the integration of complex oxides with semiconductors for a variety of applications including "smart" transistors [1] and dielectrics for high-current, high-power transistor gates [2]. While complex oxide dielectrics are now routinely integrated with silicon-based technology, examples of the marriage of complex oxide properties, including ferroelectricity, pyroelectricity, and piezoelectricity, with wide bandgap semiconductors remain rare. In this manuscript we will discuss a method to integrate the multiferroic $BiFeO_3$ by molecular beam epitaxy (MBE) with 2 wide bandgap semiconductors: SiC and AlGaN/GaN. In doing so, we will identify the necessary processing conditions and resulting crystalline properties for these exciting new device platforms.

$BiFeO_3$ has garnered tremendous recent interest due to its unique standing as the only known material possessing both ferroelectric and magnetic (antiferromagnetic) order at room temperature. Owing to its ultrahigh spontaneous polarization (~100 $\mu C \cdot cm^{-1}$) [3], [4] and high ferroelectric transition temperature ($T_c \sim 1083$ K) [5], $BiFeO_3$ is a promising material for high-temperature and high-power transistor gate applications. The high polarization provides a promising avenue to alter the carrier concentration of the 2-dimensional (2-D) electron gas channel in high electron mobility transistor (HEMT) AlGaN/GaN heterostructures. In these structures a 2-D electron gas with a $\sim 2 \times 10^{13}$ cm^{-2} sheet carrier concentration exists at the AlGaN/GaN interface [6]. To fully deplete the channel, a dielectric capable of maintaining a surface charge of ~ 3.2 $\mu C \cdot cm^{-2}$ is necessary. This value does not take into account dielectric/semiconductor interface charge trapping. This consideration suggests that a higher dielectric surface charge density is necessary. The 100 $\mu C \cdot cm^{-2}$ polarization of $BiFeO_3$ corresponds to a surface charge of $\sim 6 \times 10^{14}$ electrons$\cdot cm^{-2}$, making $BiFeO_3$ an excellent candidate.

Unlike the deposition of refractory materials by MBE where individual monolayers can be dosed to grow the crystal lattice in a layer-by-layer approach (see, for example, [7], demonstrating growth of $SrTiO_3$ by reactive MBE), the deposition of materials with volatile components requires a technique where the desorption of the volatile species is compensated by an increased partial vapor pressure of that species directly above the growth surface. By examination of the vapor pressures of the volatile gaseous species, the desired condensed phase, and the condensed volatile species, growth conditions can be identified that allow for phase-pure film growth by supplying an overpressure of the volatile components. This adsorption-controlled growth regime for MBE was first demonstrated for the III-V semiconductor GaAs where an overpressure

Manuscript received August 29, 2008; accepted December 23, 2008. This work was supported by the Office of Naval Research through Grant No. N00014-04-1-0426, monitored by Dr. Colin Wood, and by the Director, Office of Science, Office of Basic Energy Sciences, Materials Science and Engineering Division, U.S. Department of Energy under Contract No. DE-AC02-05CH11231.

J. F. Ihlefeld was with the Department of Materials Science and Engineering, Cornell University, Ithaca, NY 14853, and the Department of Materials Science and Engineering, University of California, Berkeley, CA. He is presently with Sandia National Laboratories, Albuquergue, NM (e-mail: jihlefe@sandia.gov).

W. Tian was with the Department of Materials Science and Engineering, Cornell University, Ithaca, NY 14853. He is presently with Seagate Technology, Bloomington, MN.

Z. K. Liu is with the Department of Materials Science and Engineering, The Pennsylvania State University, University Park, PA.

W. A. Doolittle is with the School of Electrical and Computer Engineering, Georgia Institute of Technology, Atlanta, GA.

M. Bernhagen, P. Reiche, and R. Uecker are with the Institute for Crystal Growth, Berlin (Adlershof), Germany.

R. Ramesh is with the Department of Materials Science and Engineering and the Department of Physics, University of California, Berkeley, CA.

D. G. Schlom is with the Department of Materials Science and Engineering, Cornell University, Ithaca, NY.

Digital Object Identifier 10.1109/TUFFC.2009.1216

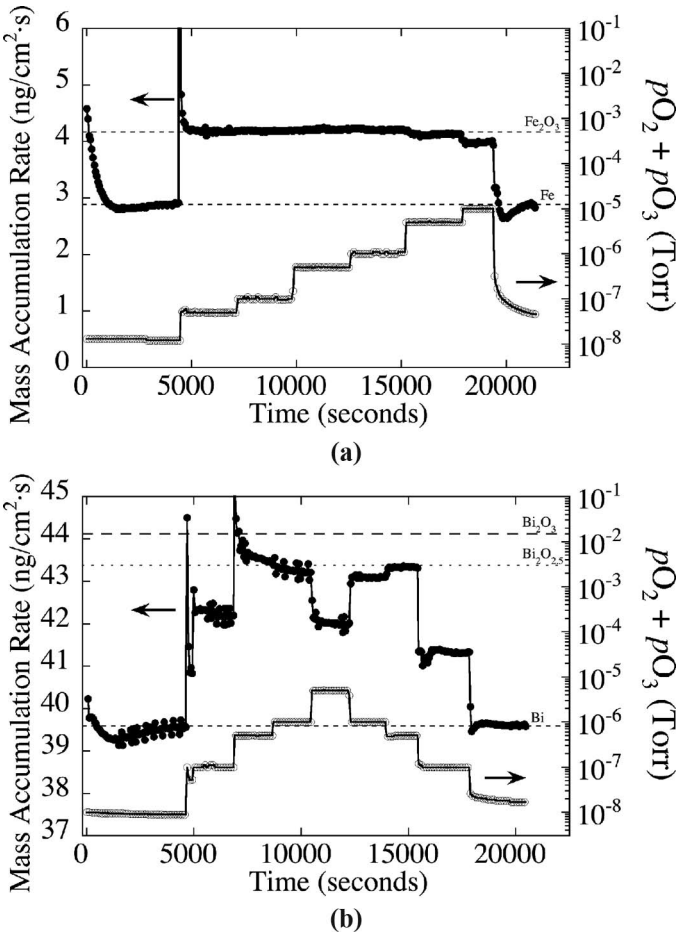

Fig. 1. Mass accumulation rate of (a) Fe_xO_y and (b) Bi_xO_y as a function of O_2 + 10% O_3 chamber background pressure.

of As_2 or As_4 gas is supplied and the film growth is controlled by the impingement rate of gallium [8]. In addition to being demonstrated for III-V semiconductors, an adsorption-controlled growth technique has been demonstrated for bismuth- [9]–[11] and lead-containing [11]–[13] ferroelectrics including, most recently, $BiFeO_3$ [14]–[16].

II. Experimental Details and Results

Films were grown within a Veeco 930 molecular beam epitaxy instrument described elsewhere [12]. To increase the local activity of oxygen without increasing the chamber pressure to an undesirable level (i.e., a level where the chamber gas limits the mean free path of the molecular beams), a gas mixture of ~10% O_3 in a balance of O_2 is supplied as the oxidizing species. Prior to film growth, boundary conditions for maximum chamber pressure were established by depositing the metallic species on a quartz crystal microbalance (QCM) inserted into the growth position [17]. The mass accumulation rate on the QCM is monitored as the O_2/O_3 mixture is introduced into the chamber and the pressure increased. An increase in the mass accumulation rate corresponds to the deposition of metal oxide species and a decrease in rate with increasing pressure corresponds to molecular-beam source oxidation or mean free path limitation. The results for depositing Fe_xO_y and Bi_xO_y are shown in Fig. 1. Upon the introduction of O_2 + O_3 into the chamber, even at the starting background O_2 + O_3 pressure of 5×10^{-8} Torr, the depositing iron immediately oxidizes to Fe_2O_3. As the pressure is increased to greater than 1×10^{-6} Torr, the mass accumulation rate decreases. This corresponds to oxidation of the iron source material and indicates that the highest useable background pressure for growth of $BiFeO_3$ in our MBE system is 10^{-6} Torr.

For the adsorption-controlled growth of the ferroelectric oxides $Bi_4Ti_3O_{12}$ and $PbTiO_3$, the necessary component thermodynamic data are readily available and have allowed for direct calculation of the adsorption-controlled growth window for phase-pure material [11], [13]. The free energy of formation of $BiFeO_3$ has yet to be experimentally determined and must be calculated to identify the necessary conditions for phase-pure deposition. As outlined in [16], the parameter space for phase-pure growth of $BiFeO_3$ was calculated using the CALPHAD method [18]. Fig. 2 shows a calculated Ellingham-type diagram representing the phase stability regions of (I) $BiFeO_3$ + γ-Fe_2O_3, (II) single-phase $BiFeO_3$, and (III) $BiFeO_3$ + $Bi_2O_{2.5}$ as a function of substrate temperature and O_2 overpressure. The boundaries between regions I, II, and III were calculated with the Gibbs energy functions of the gas phase containing various bismuth and Bi–O species and the stable and metastable iron and bismuth oxides, all taken from the SGTE database [19]. As the enthalpies of formation are not known, we consider 2 scenarios for $Bi_2O_{2.5}$ and $BiFeO_3$. The enthalpy of formation of $Bi_2O_{2.5}$ is assumed to be +100 or +4500 J/mol of $Bi_2O_{2.5}$ with respect to the Bi-Bi_2O_3 tie line. The enthalpy of formation of $BiFeO_3$ is assumed to be −1000 or −5000 J/mol of $BiFeO_3$ with respect to the Bi_2O_3-Fe_2O_3 tie line. The phase stability region was calculated using ThermoCalc [20] with the partial pressure of bismuth fixed at 6.7×10^{-10} atm. This value corresponds to the pressure at the plane of the substrate for an incident bismuth flux of 1.4×10^{14} Bi/(cm²·sec) [21]. The solid lines in Fig. 2 represent the $BiFeO_3$ phase stability region, with formation enthalpies of +100 and −1000 J/mol for $Bi_2O_{2.5}$ and $BiFeO_3$, respectively, specifying the narrowest growth window possible, whereas the dashed lines represent the stability for +4500 and −5000 J/mol, indicating the approximate uncertainty in the growth window due to the lack of relevant free energy data [16].

The thermodynamic predictions were empirically verified by growing a film while altering the growth temperature, thereby sampling a horizontal slice of the Ellingham diagram. *In situ* reflection high-energy electron diffraction (RHEED) and *ex situ* x-ray diffraction (XRD) of films grown on (001)-oriented TiO_2-terminated [22] $SrTiO_3$ substrates were used to monitor phase assemblage. A bismuth flux of 1.4×10^{14} Bi·cm^{-2}·sec^{-1}, an 8:1 Bi:Fe flux ratio, and a 1×10^{-6} Torr (O_2 + ~10% O_3) background pressure were used. Growth was initiated by supplying

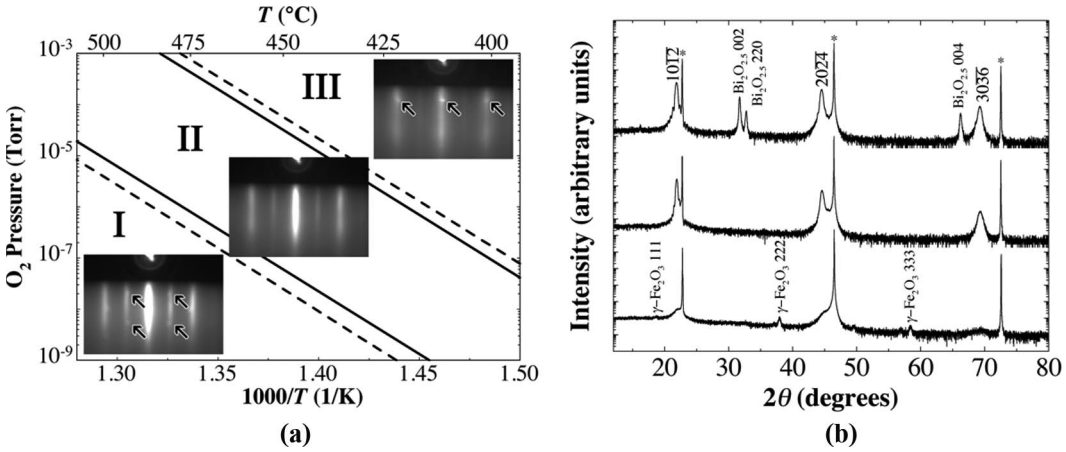

Fig. 2. (a) Calculated Ellingham diagram and reflection high-energy electron diffraction (RHEED) patterns collected along the ⟨110⟩ azimuth of $SrTiO_3$ during Bi-Fe-O deposition at different temperatures and O_2 gas overpressures. Solid lines represent phase boundaries using +100 and –1000 J/mole formula unit free energies for $Bi_2O_{2.5}$ and $BiFeO_3$, respectively, specifying the narrowest growth window possible; dashed lines represent phase boundaries for +4500 and –5000 J/mole formula unit free energies, indicating the approximate uncertainty in width of the growth window. Region I represents the phase stability region of a mixture of Bi_xO_y gases and $BiFeO_3$ and γ-Fe_2O_3 condensed phases. Region II represents the phase stability region of a mixture of Bi_xO_y gases and a $BiFeO_3$ condensed phase. Region II is the region in which phase-pure $BiFeO_3$ can be grown. Region III represents the phase stability region of a mixture of Bi_xO_y gases and $BiFeO_3$ and $Bi_2O_{2.5}$ condensed phases. Arrows on the RHEED patterns in regions I and III indicate the diffraction spots from γ-Fe_2O_3 and $Bi_2O_{2.5}$ phases, respectively. (b) X-ray diffraction patterns of films grown on (001) $SrTiO_3$ in regions I, II, and III. The asterisks (*) indicate the XRD peaks due to the (001) $SrTiO_3$ substrate. (Diagram (a) was reprinted from Ihlefeld *et al.* [16], with permission, ©2008 American Institute of Physics).

monolayer doses of the nonvolatile component iron, while oxygen/ozone and bismuth were continually supplied. In agreement with the thermodynamic calculations, at low substrate temperatures or high bismuth overpressures, a secondary $Bi_2O_{2.5}$ phase was observed to form in equilibrium with $BiFeO_3$. This secondary phase can be identified in RHEED images along a ⟨110⟩ substrate azimuth as 2 sets of 3 spots superimposed on the 01, 00, and 10 $BiFeO_3$ RHEED streaks [see arrows on the RHEED image in region III of Fig. 2(a)]. For high substrate temperatures and/or low bismuth overpressures, a secondary γ-Fe_2O_3 phase is identified as a diamond-shaped transmission RHEED pattern with 2 spots superimposed on the $BiFeO_3$ half-order streaks and single spots on the 01 and 10 $BiFeO_3$ streaks [see arrows on the RHEED image in region I of Fig. 2(a)]. The corresponding substrate temperatures for the appearance of $Bi_2O_{2.5}$ and γ-Fe_2O_3 for the given growth conditions were approximately 415°C and 460°C, respectively, as measured via band-edge spectroscopy [23], [24]. Phase-pure $BiFeO_3$ films can be grown at intermediate temperatures. Fig. 2 shows the RHEED and XRD patterns for films grown in each of the 3 growth regimes, with the RHEED data superimposed on the corresponding growth regimes. Note that hexagonal indices are used throughout this manuscript to index the $BiFeO_3$ XRD spectra [25].

With the parameters for phase-pure growth established, a 75-nm-thick film was deposited on (101)-oriented $DyScO_3$ under conditions allowing for single-phase $BiFeO_3$ (the standard crystallographic setting of $DyScO_3$, space group #62 (*Pnma*), are used in this manuscript). XRD patterns for this film are shown in Fig. 3. No diffraction features attributed to secondary phases are identified in the θ-2θ scans. High-resolution ω-rocking curves were collected for the $BiFeO_3$ $20\overline{2}\overline{4}$ and $DyScO_3$ 202 diffraction peaks, as shown in Fig. 3(b). Full width at half maximum (FWHM) values of 7.2 arc sec (0.002 degrees) were obtained for both, indicating that the film crystallinity is substrate limited. This value represents a fourfold improvement over the narrowest reported value in the literature for $BiFeO_3$ films grown by MBE [15], and a 160-fold improvement over the narrowest reported by other techniques [26]; it is among the narrowest recorded for any complex oxide thin film [27], [28]. These narrow rocking curve values suggest low dislocation concentrations, which may lead to improved electrical response [29]–[32].

It is known that many perovskites [33]–[36] and cubic symmetry oxides with similar lattice parameters [37]–[41] grow in a $(111)_p$ orientation (where the p subscript denotes pseudocubic notation) on the basal plane of many hexagonal wide bandgap semiconductors, including GaN and SiC. Therefore, we have investigated the growth of $BiFeO_3$ in this orientation by depositing a 75-nm-thick film on (011)-oriented $DyScO_3$ [note that this orientation is $(111)_p$-type]. Fig. 4 shows the XRD data for the as-grown film. As with the $(001)_p$-oriented films, phase-pure material is identified. Similar to films grown on (111) $SrTiO_3$ [15], a (0001) orientation is identifed. This is significant because the ferroelectric polar axis is perpendicular to the (0001) planes in $BiFeO_3$ and suggests that the ~100 $\mu C \cdot cm^{-2}$ polarization is oriented normal to the substrate plane. X-ray ω-rocking curves again reveal substrate-limited crystallinity.

To minimize surface contaminants [42], AlGaN/GaN heterostructure substrates were prepared by exposure to 1:1 HCl:H_2O and 1:99 H_2O:HF pretreatments followed by

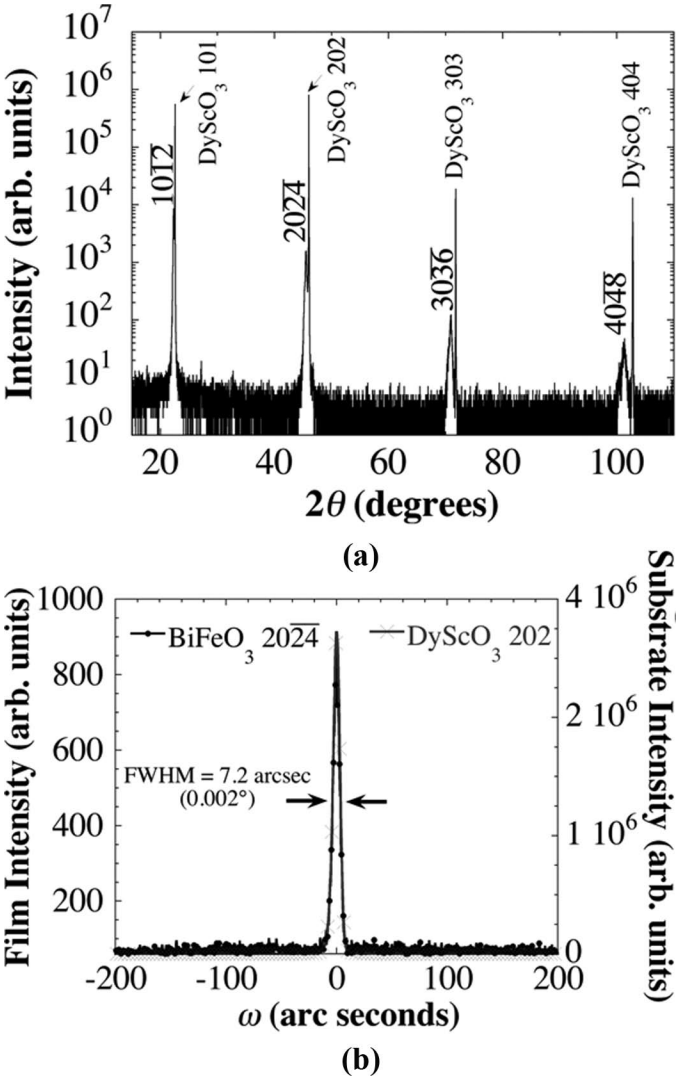

Fig. 3. (a) θ-2θ x-ray diffraction pattern of a 75-nm-thick epitaxial $BiFeO_3$ film deposited on (101) $DyScO_3$; (b) ω-rocking curves of $BiFeO_3$ $20\bar{2}4$ and $DyScO_3$ 202 diffraction peaks.

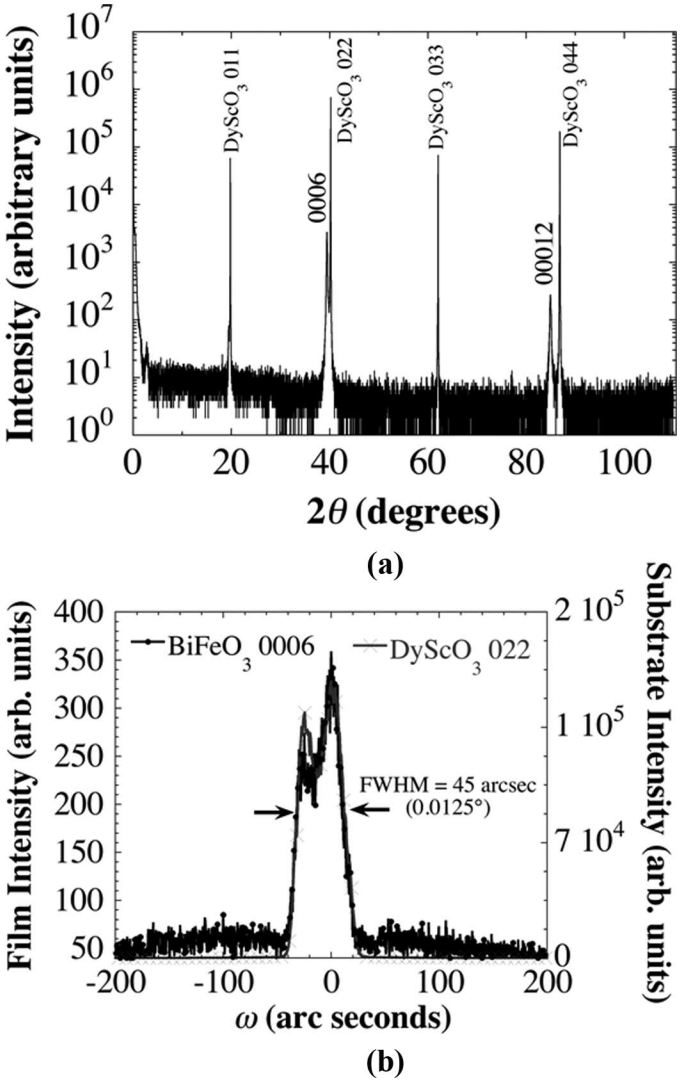

Fig. 4. (a) θ-2θ x-ray diffraction pattern of a 75-nm-thick epitaxial $BiFeO_3$ deposited on (011) $DyScO_3$; (b) ω-rocking curves of $BiFeO_3$ 0006 and $DyScO_3$ 022 diffraction peaks.

H_2O rinses before introduction into the growth chamber. On these subsrates, $SrTiO_3/TiO_2$ films were formed by depositing 5 monolayers of (100)-oriented TiO_2 [43] and subsequently capping with 4 monolayers of SrO at 600°C and in a 1×10^{-6} Torr O_2 background pressure. These layers react to form (111)-oriented $SrTiO_3$, as shown in the reflection high-energy electron diffraction patterns collected along the AlGaN $\langle 11\bar{2}0 \rangle$ azimuthal direction in Fig. 5. Films were allowed to cool to approximately 420°C, and the background atmosphere was altered to include 10% ozone before $BiFeO_3$ growth. Fig. 6 shows θ-2θ and azimuthal ϕ XRD scans for 75-nm $BiFeO_3$/2-nm $SrTiO_3$/ <1-nm TiO_2/(0001) AlGaN/GaN grown by MBE. Only diffraction peaks attributed to the substrate and dielectric heterostructure stacks are present, with no secondary phases. The $BiFeO_3$ film is predominantly (0001)-oriented. The presence of the $2\bar{2}02$ peak indicates approximately 3% out-of-plane twinning, as calculated by peak intensity ratios. It is important to note that the $2\bar{2}02$ peak is of the same 111-pseudocubic family as the 0006 peak; however, only the (0001) plane is perpendicular to the ferroelectric polar axis and the substrate surface. These $\left(1\bar{1}01\right)$ $BiFeO_3$ twins have also been observed in strain-relaxed $BiFeO_3$ grown on (111) $SrTiO_3$ [44]. As was observed in films deposited by chemical vapor deposition, an in-plane orientation relationship of $\left[11\bar{2}0\right]$ $BiFeO_3$ || $\left[11\bar{2}0\right]$ AlGaN plus an additional 180° twin variant is present [33]. The 180° vari-

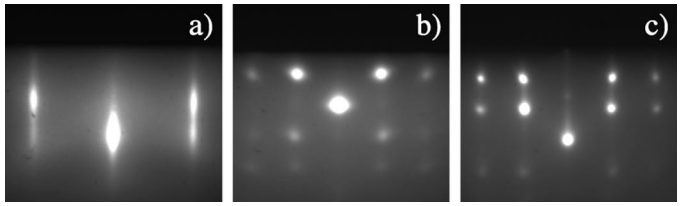

Fig. 5. Reflection high-energy electron diffraction (RHEED) patterns collected along the $\langle 11\bar{2}0 \rangle$ AlGaN/GaN direction of (a) AlGaN, (b) 2-nm $SrTiO_3$, and (c) 75-nm $BiFeO_3$.

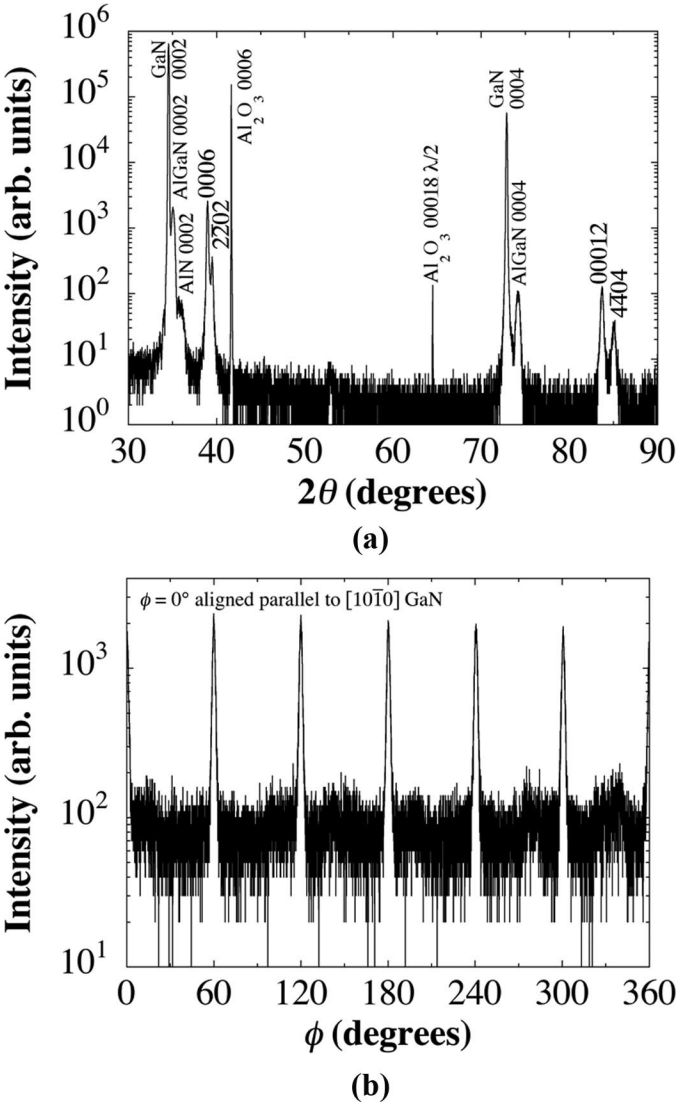

Fig. 6. (a) θ-2θ x-ray diffraction pattern of 75-nm-thick epitaxial $BiFeO_3$ deposited on (0001) AlGaN/GaN; (b) azimuthal ϕ-scan of $BiFeO_3$ $10\bar{1}\bar{2}$.

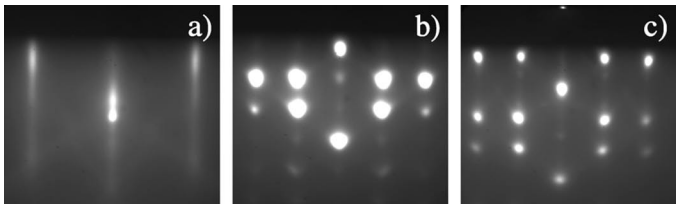

Fig. 7. Reflection high-energy electron diffraction (RHEED) patterns collected along the $\langle 11\bar{2}0 \rangle$ SiC direction of (a) SiC, (b) 2-nm $SrTiO_3$, and (c) 30-nm $BiFeO_3$.

ant forms during the reaction to form $SrTiO_3$ and is inherited by the epitaxial $BiFeO_3$ overlayer.

Intervening $SrTiO_3/TiO_2$ layers have also allowed successful integration of $BiFeO_3$ with (0001) 6H-SiC. The dielectric heterostructure layers were deposited in the same manner as the films on GaN. Fig. 7 shows the RHEED patterns collected along the $\langle 11\bar{2}0 \rangle$ azimuth of SiC throughout the growth sequence from bare SiC to 2-nm

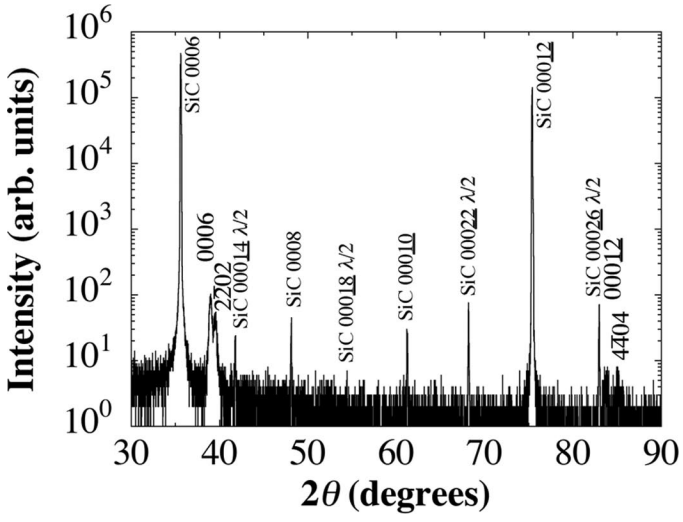

Fig. 8. θ-2θ x-ray diffraction pattern of a 30-nm-thick epitaxial $BiFeO_3$ film deposited on (0001) SiC.

$SrTiO_3$ and 30-nm $BiFeO_3$. As evident in the XRD patterns in Fig. 8, the (0001)-$BiFeO_3$ orientation dominates, indicating that the polar axis is perpendicular to the substrate surface. The presence of the $2\bar{2}02$ $BiFeO_3$ peak indicates approximately 3% out-of-plane twinning, as calculated by peak intensity ratios. RHEED patterns collected along the $\langle 11\bar{2}0 \rangle$ and $\langle 10\bar{1}0 \rangle$ substrate azimuths indicate that the 180° in-plane twin variant is present in these $BiFeO_3$/SiC films, just as it was present in $BiFeO_3$/GaN films [33].

III. Conclusions

We have demonstrated the growth of $BiFeO_3$ on several oxide and wide bandgap semiconductor substrates using reactive molecular beam epitaxy in an adsorption-controlled growth regime. This work represents an important step in the successful preparation of high-power, high-temperature electronic devices where transistor channel characteristics can be altered by a ferroelectric gate. Ongoing work is being conducted on device fabrication including the incorporation of wide-bandgap perovskite oxides in the dielectric stack to reduce leakage currents due to electron tunneling [45].

References

[1] Y.-R. Wu and J. Singh, "Polar heterostructure for multifunction devices: Theoretical studies," *IEEE Trans. Electron. Devices*, vol. 52, pp. 284–293, 2005.

[2] W. A. Doolittle, G. Namkoong, A. G. Carver, and A. S. Brown, "Challenges and potential payoff for crystalline oxides in wide bandgap semiconductor technology," *Solid-State Electron.*, vol. 47, pp. 2143–2147, 2003.

[3] J. Wang, J. B. Neaton, H. Zheng, V. Nagarajan, S. B. Ogale, B. Liu, D. Viehland, V. Vaithyanathan, D. G. Schlom, U. V. Waghmare, N. A. Spaldin, K. M. Rabe, M. Wuttig, and R. Ramesh, "Epitaxial $BiFeO_3$ multiferroic thin film heterostructures," *Science*, vol. 299, pp. 1719–1722, 2003.

[4] J. F. Li, J. L. Wang, M. Wuttig, R. Ramesh, N. Wang, B. Ruette, A. P. Pyatakov, A. K. Zvezdin, and D. Viehland, "Dramatically enhanced polarization in (001), (101), and (111) $BiFeO_3$ thin films

due to epitiaxial-induced transitions," *Appl. Phys. Lett.*, vol. 84, pp. 5261–5263, 2004.
[5] G. A. Smolenskii and I. E. Chupis, "Ferroelectromagnets," *Sov. Phys. Usp.*, vol. 25, pp. 475–493, 1982.
[6] S. Arulkumaran, T. Egawa, H. Ishikawa, and J. Jimbo, "Characterization of different-Al-content $Al_xGa_{1-x}N$/GaN heterostructures and high-electron-mobility transistors on sapphire," *J. Vac. Sci. Technol. B*, vol. 21, pp. 888–894, 2003.
[7] J. H. Haeni, C. D. Theis, and D. G. Schlom, "RHEED intensity oscillations for the stoichiometric growth of $SrTiO_3$ thin films by reactive molecular beam epitaxy," *J. Electroceram.*, vol. 4, pp. 385–391, 2000.
[8] J. R. Arthur, "Interaction of Ga and As_2 molecular beams with GaAs surfaces," *J. Appl. Phys.*, vol. 39, pp. 4032–4034, 1968.
[9] C. D. Theis, J. Yeh, D. G. Schlom, M. E. Hawley, G. W. Brown, J. C. Jiang, and X. Q. Pan, "Adsorption-controlled growth of $Bi_4Ti_3O_{12}$ by reactive MBE," *Appl. Phys. Lett.*, vol. 72, pp. 2817–2819, 1998.
[10] S. Migita, H. Ota, H. Fujino, Y. Kasai, and S. Sakai, "Epitaxial $Bi_4Ti_3O_{12}$ thin film growth using Bi self-limiting function," *J. Cryst. Growth*, vol. 200, pp. 161–168, 1999.
[11] D. G. Schlom, J. H. Haeni, J. Lettieri, C. D. Theis, W. Tian, J. C. Jiang, and X. Q. Pan, "Oxide nano-engineering using MBE," *Mater. Sci. Eng. B*, vol. 87, pp. 282–291, 2001.
[12] C. D. Theis and D. G. Schlom, "Epitaxial lead titanate grown by MBE," *J. Cryst. Growth*, vol. 174, pp. 473–479, 1997.
[13] C. D. Theis, J. Yeh, D. G. Schlom, M. E. Hawley, and G. W. Brown, "Adsorption-controlled growth of $PbTiO_3$ by reactive molecular beam epitaxy," *Thin Solid Films*, vol. 325, pp. 107–114, 1998.
[14] J. Kabelac, S. Ghosh, P. S. Dobal, and R. Katiyar, "RF oxygen plasma assisted molecular beam epitaxy growth of $BiFeO_3$ thin films on $SrTiO_3$ (001)," *J. Vac. Sci. Technol. B*, vol. 25, pp. 1049–1052, 2007.
[15] J. F. Ihlefeld, A. Kumar, V. Gopalan, D. G. Schlom, Y. B. Chen, X. Q. Pan, T. Heeg, J. Schubert, X. Ke, P. Schiffer, J. Orenstein, L. W. Martin, Y. H. Chu, and R. Ramesh, "Adsorption-controlled molecular-beam epitaxial growth of $BiFeO_3$," *Appl. Phys. Lett.*, vol. 91, art. no. 071922, 2007.
[16] J. F. Ihlefeld, N. J. Podraza, Z. K. Liu, R. C. Rai, X. Xu, T. Heeg, Y. B. Chen, J. Li, R. W. Collins, J. L. Musfeldt, X. Q. Pan, J. Schubert, R. Ramesh, and D. G. Schlom, "Optical band gap of $BiFeO_3$ grown by molecular-beam epitaxy," *Appl. Phys. Lett.*, vol. 92, art. no. 142908, 2008.
[17] C. D. Theis and D. G. Schlom, "The reactivity of ozone incident onto the surface of perovskite thin films grown by MBE," in *High Temperature Materials Chemistry IX*, vol. 97–39, K. E. Spear, Ed. Pennington, NJ: Electrochemical Society, 1997, pp. 610–616.
[18] L. Kaufman, "Computational thermodynamics and materials design," *CALPHAD (Computer Coupling of Phase Diagrams and Thermochemistry)*, vol. 25, pp. 141–161, 2001.
[19] Scientific Group Thermodata Europe (SGTE), "Thermodynamic properties of inorganic materials," in *Landolt-Börnstein New Series, Group IV*, vol. 19, Lehrstuhl für Theoretische Hüttenkunde, Ed. Berlin, Heidelberg: Springer, 1999.
[20] J. O. Andersson, T. Helander, L. H. Hoglund, P. F. Shi, and B. Sundman, "THERMO-CALC & DICTRA, computational tools for materials science," *CALPHAD (Computer Coupling of Phase Diagrams and Thermochemistry)*, vol. 26, pp. 273–312, 2002.
[21] D. G. Schlom and J. S. J. Harris, "MBE Growth of High T_c Superconductors," in *Molecular Beam Epitaxy: Applications to Key Materials*, R. F. C. Farrow, Ed. Park Ridge, N.J.: Noyes Publications, 1995, pp. 505–622.
[22] G. Koster, B. L. Kropman, G. J. H. M. Rijnders, D. H. A. Blank, and H. Rogalla, "Quasi-ideal strontium titanate crystal surfaces through formation of strontium hydroxide," *Appl. Phys. Lett.*, vol. 73, pp. 2920–2922, 1998.
[23] E. S. Hellman and J. S. Harris, "Infra-red transmission spectroscopy of GaAs during molecular-beam epitaxy," *J. Cryst. Growth*, vol. 81, pp. 38–42, 1987.
[24] kSA BandiT datasheet, k-Space Associates, Inc., Ann Arbor, MI.
[25] F. Kubel and H. Schmid, "Structure of a ferroelectric and ferroelastic monodomain crystal of the perovskite $BiFeO_3$," *Acta Crystallogr. B*, vol. B46, pp. 698–702, 1990.
[26] R. R. Das, D. M. Kim, S. H. Baek, C. B. Eom, F. Zavaliche, S. Y. Yang, R. Ramesh, Y. B. Chen, X. Q. Pan, X. Ke, M. S. Rzchowski, and S. K. Streiffer, "Synthesis and ferroelectric properties of epitaxial $BiFeO_3$ thin films grown by sputtering," *Appl. Phys. Lett.*, vol. 88, art. no. 242904, 2006.
[27] M. D. Biegalski, D. D. Fong, J. A. Eastman, P. H. Fuoss, S. K. Streiffer, T. Heeg, J. Schubert, W. Tian, C. T. Nelson, X. Q. Pan, M. E. Hawley, M. Bernhagen, P. Reiche, R. Uecker, S. Trolier-McKinstry, and D. G. Schlom, "Critical thickness of high structural quality $SrTiO_3$ films grown on orthorhombic (101) $DyScO_3$," *J. Appl. Phys.*, vol. 104, art. no. 114109, 2008.
[28] M. D. Biegalski, Y. Jia, D. G. Schlom, S. Trolier-McKinstry, S. K. Streiffer, V. Sherman, R. Uecker, and P. Reiche, "Relaxor ferroelectricity in strained epitaxial SrTiO3 thin films on DyScO3 substrates," Appl. Phys. Lett., vol. 88, art. no. 192907, 2006.
[29] S. P. Alpay, I. B. Misirlioglu, V. Nagarajan, and R. Ramesh, "Can interface dislocations degrade ferroelectric properties?" *Appl. Phys. Lett.*, vol. 85, pp. 2044–2046, 2004.
[30] M. W. Chu, I. Szafraniak, R. Scholz, C. Harnagea, D. Hesse, M. Alexe, and U. Gosele, "Impact of misfit dislocations on the polarization instability of epitaxial nanostructured ferroelectric perovskites," *Nat. Mater.*, vol. 3, pp. 87–90, 2004.
[31] V. Nagarajan, C. L. Jia, H. Kohlstedt, R. Waser, I. B. Misirlioglu, S. P. Alpay, and R. Ramesh, "Misfit dislocations in nanoscale ferroelectric heterostructures," *Appl. Phys. Lett.*, vol. 86, art. no. 192910, 2005.
[32] Y. L. Li, S. Y. Hu, S. Choudhury, M. I. Baskes, A. Saxena, T. Lookman, Q. X. Jia, D. G. Schlom, and L. Q. Chen, "Influence of interfacial dislocations on hysteresis loops of ferroelectric films," *J. Appl. Phys.*, vol. 104, art. no. 104110, 2008.
[33] W. Tian, V. Vaithyanathan, D. G. Schlom, Q. Zhan, S. Y. Yang, Y. H. Chu, and R. Ramesh, "Epitaxial integration of (0001) $BiFeO_3$ with (0001) GaN," *Appl. Phys. Lett.*, vol. 90, art. no. 172908, 2007.
[34] S. Y. Yang, Q. Zhan, P. L. Yang, M. P. Cruz, Y. H. Chu, R. Ramesh, Y. R. Wu, J. Singh, W. Tian, and D. G. Schlom, "Capacitance-voltage characteristics of $BiFeO_3/SrTiO_3$/GaN heteroepitaxial structures," *Appl. Phys. Lett.*, vol. 91, art. no. 022909, 2007.
[35] S. K. Dey, W. Cao, S. Bhaskar, and J. Li, "Highly textured $Pb(Zr_{0.3}Ti_{0.7})O_3$ thin films on GaN/sapphire by metalorganic chemical vapor deposition," *J. Mater. Res.*, vol. 21, pp. 1526–1531, 2006.
[36] C. R. Cho, J. Y. Hwang, J. P. Kim, S. Y. Jeong, S. G. Yoon, and W. J. Lee, "Growth and characterization of (Ba0.5Sr0.5)TiO3 films epitaxially grown on (002) GaN/(0006) Al2O3 electrode," Jpn. J. Appl. Phys., vol. 43, pp. L1425–L1428, 2004.
[37] H. S. Craft, R. Collazo, M. D. Losego, S. Mita, Z. Sitar, and J. P. Maria, "Spectroscopic analysis of the epitaxial CaO (111)-GaN (0002) interface," *Appl. Phys. Lett.*, vol. 92, art. no. 082907, 2008.
[38] H. S. Craft, J. F. Ihlefeld, M. D. Losego, R. Collazo, Z. Sitar, and J. P. Maria, "MgO epitaxy on GaN (0002) surfaces by molecular beam epitaxy," *Appl. Phys. Lett.*, vol. 88, art. no. 212906, 2006.
[39] M. D. Losego, S. Mita, R. Collazo, Z. Sitar, and J. P. Maria, "Epitaxial growth of the metastable phase ytterbium monoxide on gallium nitride surfaces," *J. Cryst. Growth*, vol. 310, pp. 51–56, 2008.
[40] T. L. Goodrich, Z. Cai, M. D. Losego, J. P. Maria, and K. S. Ziemer, "Thin, crystalline MgO on hexagonal 6H-SIC(0001) by molecular beam epitaxy for functional oxide integration," *J. Vac. Sci. Technol. B*, vol. 25, pp. 1033–1038, 2007.
[41] A. Schmehl, V. Vaithyanathan, A. Herrnberger, S. Thiel, C. Richter, M. Liberati, T. Heeg, M. Rockerath, L. F. Kourkoutis, S. Muhlbauer, P. Boni, D. A. Muller, Y. Barash, U. Schubert, Y. Idzerda, J. Mannhart, and D. G. Schlom, "Epitaxial integration of the highly spin-polarized ferromagnetic semiconductor EuO with silicon and GaN," *Nat. Mater.*, vol. 6, pp. 882–887, 2007.
[42] L. L. Smith, S. W. King, R. J. Nemanich, and R. F. Davis, "Cleaning of GaN surfaces," *J. Electron. Mater.*, vol. 25, pp. 805–810, 1996.
[43] P. J. Hansen, V. Vaithyanathan, Y. Wu, T. Mates, S. Heikman, U. K. Mishra, R. A. York, D. G. Schlom, and J. S. Speck, "Rutile films grown by molecular beam epitaxy on GaN and AlGaN/GaN," *J. Vac. Sci. Technol. B*, vol. 23, pp. 499–506, 2005.
[44] J. F. Ihlefeld, A. Kumar, X. Q. Pan, V. Gopalan, D. G. Schlom, and R. Ramesh, "Symmetry, strain relaxation, and crystallographic twinning in epitaxial $BiFeO_3$ thin films on (111) $SrTiO_3$," to be published.
[45] J. F. Ihlefeld, H. S. Craft, T. Heeg, R. Collazo, S. Mita, Z. Sitar, J.-P. Maria, R. Ramesh, and D. G. Schlom, "Band offsets of SrTiO3, GdScO3/SrTiO3, and LaAlO3/SrTiO3 epitaxial heterostructures with (0001) GaN," to be published.

The authors' photos and biographies were unavailable at time of publication.